Sensing and Bio-Sensing Research 48 (2025) 100777

Contents lists available at ScienceDirect

Sensing and Bio-Sensing Research

journal homepage: www.elsevier.com/locate/sbsr

Microneedle-based electrochemical sensors for real-time pH and sodium monitoring in physiological environments

Fahima Rahman [a], Adam Ryan [b], Andrea Bocchino [c], Paul Galvin [c], Sofia Rodrigues Teixeira [c,*]

[a] School of Chemistry, University College Cork, Ireland
[b] School of Biochemistry and cell biology, University College Cork, Ireland
[c] Tyndall National Institute, University College Cork, Lee Maltings, Cork, Ireland

ARTICLE INFO

Keywords:
Microneedles
pH
Sodium
ISF
Electrochemistry

ABSTRACT

This study proposes developing microneedle (MN) sensors for pH and sodium detection. MNs are minimally invasive, miniaturized needles capable of piercing the stratum corneum to access dermal interstitial fluid (ISF). They can offer accessible, quick, and precise point-of-care diagnostics, potentially replacing centralized laboratory testing. The study uses electrochemical techniques for sensor modification, detection, and in-vitro characterizations. This work aimed to create and validate a polymer-based disposable microneedle patch for future transdermal electrochemical sensing. Successful potentiometric sensor development for pH detection using SiOx as passivation layers with IrOx functionalization was demonstrated. Additionally, voltametric sodium sensors were achieved with ARcare passivation and PEDOT functionalization. Both pH and Na^+ sensors exhibited linear responses within normal physiological levels across various solutions. The pH sensors showed sensitivity of −60.5 mV/pH and an accuracy of 97.7 % alongside an error margin of 2.3 %, while sodium sensors achieved a sensitivity of 3.29 nA/mM/mm^2. Both sensors exhibit dynamic, rapid responses, along with good repeatability, stability, and selectivity. Over a twenty-one-day span for pH sensors and a fourteen-day period for sodium sensors, this study offers validation that microneedles serve as a viable foundation for wearable systems, enabling real-time, multiparameter biosensing of interstitial fluids.

1. Introduction

In recent years, the intersection of electrochemical sensing and biomedical technologies has yielded groundbreaking advancements, with microneedles emerging as a focal point in this innovative landscape. Microneedle-based sensors have evolved into powerful tools for real-time monitoring of physiological parameters, particularly within the interstitial fluid.

The significance of pH [1–3] and sodium [4,5] as vital indicators of physiological homeostasis show the importance of accurate and reliable monitoring methods. Traditional methods face limitations in providing continuous, minimally invasive monitoring, creating a demand for advanced biosensing technologies. Microneedle-based sensors, with their minimally invasive nature and ability to penetrate the skin's outer layers, offer a promising option for continuous monitoring of biochemical changes in real time [2,6–8].

Results from numerous studies have highlighted a significant demand for pH measurements [1–3]. Lee et al. [3] developed a sensor for monitoring pH to understand the tissue damage caused by ischemic symptoms, for this they measured pH value by PANI and Ag/AgCl electrochemically deposited on the open window of the microneedle, which is widely used to fabricate biochemical sensors [3]. Thus, monitoring the changes to pH in vivo has a significant clinical significance which is recognised by a number of authors [1–3]. Guzmán et al. [2] discussed literature published regarding pH sensing microneedles. Mani et al. [9] developed a pH sensor in cerebrospinal fluid. Zuliani et al. [10] designed an iridium oxide sensor for mapping pH distributions in rat heart. Zhou et al [11]. designed a pH sensor with PANI functionalised acupuncture needles for real time monitoring of pH changes in the brain [2]. Guzmán et al. [2] have identified that these previous studies have not covered the determination of pH in interstitial fluid. They presented a pH MN sensor for the transdermal pH determination in rat ISF. This suggests a research gap in terms of monitoring pH in interstitial fluid.

Table 1 provides a summary of microneedle sensors for pH detection, allowing for a comparison with our own study.

Electrolytes play a critical role in many key physicochemical

* Corresponding author.
E-mail address: sofia.teixeira@tyndall.ie (S.R. Teixeira).

https://doi.org/10.1016/j.sbsr.2025.100777
Received 15 January 2025; Received in revised form 11 March 2025; Accepted 12 March 2025
Available online 14 March 2025

functions, such as hydration, muscle activation, active membrane transport, and many others [20–22]. Electrolyte imbalances can lead to various perturbations, such as hyperkalemia, hypernatremia, hypokalemia, and hyponatremia, which in turn could lead to a range of clinical conditions such as arrhythmias, mental status changes including seizures, muscle cramps, and even death [23,24]. Sodium is one of the most abundant molecules within the human body that plays a vital role in a range of cellular functionality, therefore it is of the upmost importance that sodium concentrations remain consistent to ensure normal physiological functioning [4,5]. Li et al. [25] created a microneedle sensor to continuously monitor Na^+ and K^+ levels in skin ISFs. Their research demonstrated the use of stainless-steel hollow microneedles with a length of 4 mm (outer diameter: 0.464 mm, inner diameter: 0.260 mm) to measure Na^+ and K^+ in artificial interstitial fluid.

Table 2 provides a summary of sodium sensors documented in the literature, offering a comparison with our study.

This paper shows the process of fabrication and implementing microneedle sensors for pH and sodium detection in the challenging environment of ISF. This platform can be used as a multiparametric sensor for the development of wearable biosensing systems, for personalized healthcare and diagnostics creating point of care devices.

2. Experimental

2.1. Materials

Phosphate buffered saline (PBS), ferrocenecarboxylic acid (FcCOOH), Hydrogen peroxide (H_2O_2 0.5 mL; 30 %), oxalic acid dehydrate (~250 mg), potassium carbonate and Poly(3,4-ethylenedioxythiophene) (PEDOT) were obtained from Sigma Aldrich. Buffer pH solutions were purchased from Centipur. Iridium (IV) chloride was purchased from Alfa-Aesar (Massachusetts, United States). For the production of the mould, 184 Silicone Elastomer Base and 184 Silicone Elastomer curing agent was purchased from The Dow Chemical Company (Midland, Michigan, United States). For microneedle wafer production, Epotek 353ND Kit Part A and B was purchased from Epoxy Technology. 8830S-Silver conductive epoxy adhesive glue was purchased from MG Chemicals. Synthetic ISF was prepared by combining 5 mM $CaCl_2$, 10 mM Hepes, 3.5 mM KCl, 0.7 mM $MgSO_4$, 123 mM NaCl, 1.5 mM NaH_2PO_4, 7.4 mM saccharose. This solution was adjusted to pH 7.5 [25,29]. 0.01 M of PEDOT was dissolved in 0.1 M KCl. A 1 mM ferrocene carboxylic acid solution was prepared in 10 mM PBS. All solutions were prepared with double distilled 18.2 MΩ deionized water.

2.2. Electrochemical setup

Electrochemical measurements were conducted with a potentiostat/galvanostat, Metrohm Autolab, PGSTAT100 controlled by Nova software (Metrohm, Cheshire, UK). All experiments were performed at room temperature using a Faraday Cage. A three-electrode cell was used for electrochemical characterisation, the MN array electrode was used as a working electrode (WE) versus an external Ag/AgCl RE (Gamry) and an external Pt (Gamry) counter electrode. Cyclic voltammetry (CV) was used to characterize the microneedle working electrodes.

2.3. Microneedle arrays

The microneedle arrays used in this study were previously developed in our research [30]. Epoxy microneedles were moulded to form 9 mm circular arrays. The needles were 500 μm tall and with a tip-to-tip pitch of 1.75 mm. 20 nm of titanium (Ti) and 100 nm of platinum (Pt) were metallized, using a Quorum Q300T D Plus, on the front and back of the arrays. The base area between the needles was then passivated either by sputtering 600 nm of SiO_2 or applying a patterned medical grade tape (ARcare 7759 from Adhesive Research cut with a Graphtec 7000–40CE vinyl cutter). Respectively, the passivation layers left 1×1 mm^2 squares and 500 μm circles exposed around the needle and centred on the needle tips. Finally, all arrays were mounted on 3D printed supports (white resin from Formlabs printed with a Formlab 3 printer) and readied for electrochemical testing.

2.4. Electrodes cleaning

For the cleaning of the microneedle electrodes, CV scans were performed to remove contaminants. CV measurements were performed in 10 mM of PBS and 1 mM of FcA with a potential ranging from −0.5 to +0.5 V at a scan rate of 0.15 V/s. An acid clean was performed with H_2O_2 for 10 scans with a potential ranging from 0 to +0.6 V at a scan

Table 1
Current pH MN sensors developed.

Biomarker	Modification	Technique	Sensitivity	Type of MN	Ref
pH	PANI	Potentiometry	94 mV/pH	Polymer MNs	[3]
pH in mouse cerebrospinal fluid and bladder	Deposition of ZnO thin films	Potentiometry	−46.35 mV/pH	Tungsten MNs	[9]
pH for on-body measurements in rats	Carbon ink, hydrogen-selective membrane	Potentiometry	54.4 mV/dec	Stainless steel solid MNs	[10]
pH	MoS_2 nanosheets and PANI	Potentiometry	−51.2 mV/pH	Acupuncture microneedles	[11]
pH	Unmodified carbon-polystyrene microneedle patch	Potentiometry	$E_{pa}/V = -0.0575$ pH + 0.4107	Carbon composite microneedle sensors	[12]
pH, lactate, and glucose	Carbon paste microneedle platforms	Potentiometry		Hollow microneedle array	[13]
pH	Iridium Oxide	Potentiometry	48 ± 11 mV/pH	Polycarbonate microneedle	[14]
pH	MNs coated with PANI coated onto the CNT/CNC@Ag film	Potentiometry and Impedance	pH in the linear range of 3–10.	Stainless steel (SS) MNs	[15]
pH	MN electrodes were modified with PANI	Potentiometry	59 mV/pH, with a range of 5–9	Hollow microneedle	[16]
pH	Gold-coated MN covered with a monolayer of 1-hexanethio	Potentiometry	−56.9 ± 0.5 mV/decade for CIM carbon, − 54.7 ± 4.1 mV/decade for MCN, −55.9 ± 3.1 mV/decade for SPC, with linear pH 4.5–11.2	Stainless steel	[17]
pH	MN-based sensor array	Potentiometry	50.4 mV/dec, with a range of 5–8.5	Stainless steel	[18]
pH	Solid microneedle array with polyaniline as a pH-sensitive layer.	Potentiometry	−59.9 ± 1.5 mV/pH	3D-printed	[19]
pH	MNs coated with Iridium Oxide	Potentiometry	−60.5 mV/pH, with a range of 3–11	Polymer-based MN	This work

Table 2
Current sodium MN developed.

Biomarker	Modification	Technique	Sensitivity	Type of MN	Ref
Na^+	Na^+ selective membrane, polyaniline (PANI)	Field Effect transistor (FET) transducer	LOD = 2780 nM	Polymer MNs	[4]
Na^+	Na^+ selective membrane and Poly (3,4-ethylenedioxythiophene) (PEDOT)	Potentiometry	50.03 mV/decade	Stainless-steel hollow MN	[25]
Na^+	Na^+ selective membrane, PEDOT and POT	Potentiometry	52.4 ± 6.3 mV/decade	Wearable sensor	[26]
Na^+	Na^+ selective membrane	Potentiometry	60.0 ± 4.0 mV/decade	Screen printed sensor	[27]
Na^+	Na^+ selective membrane	Potentiometry	–	Wearable MIMN Patch	[28]
Na^+	Na^+ selective membrane	SWV	LOD = 13.3 pM	Polymer based MNs	This work

rate of 0.15 V/s.

2.5. Electrodeposition of IrOx solution onto the sensor surface

The electrodeposition solution was prepared following the method outlined by Yamanaka [31]. Initially, iridium (IV) chloride hydrate ($IrCl_4{\cdot}H_2O$) was dissolved in deionized water under magnetic stirring for 30 min. Subsequently, 1 mL of aqueous 30 % H_2O_2 was added to the solution and stirring continued for an additional 30 min. Afterward, 0.5 g of oxalic acid ($C_2H_2O_4$) was introduced, and the solution was stirred for another 30 min. The pH of the solution was adjusted to approximately 10 by the addition of Na_2CO_3. The stabilized solution was kept at room temperature, with its colour transitioning from light yellow to dark blue, and no precipitation was observed at the solution bottle's bottom.

For the electrodeposition of IrOx onto the sensor surface, varying numbers of cyclic voltammetry (CV) scans were applied, using a potential range from −0.7 to +0.7 V at a scan rate of 0.1 V/s. Specifically, 10 scans were required for SiO_2 electrode modification.

2.6. PEDOT electropolymerisation

A chronoamperometry technique was utilized to deposit a PEDOT film at a consistent potential of 1 V in a three-electrode electrochemical cell. PEDOT films were created through a single continuous polymerization step in a solution containing 0.01 M PEDOT in 0.1 M KCl, with polymerization time set at 30 s. Various times and deposition processes were evaluated before determining the most appropriate one for this procedure. The tests were conducted at room temperature under light exposure.

2.7. Depositing of the sodium ion-selective membrane

A sodium ion-selective membrane (ISM) was formed on a MN Pt electrode. The sodium-ISM cocktail was prepared by mixing Na ionophore X (1 % *w*/w), Na-TFPB (0.55 % w/w), DOS (65.45 % w/w), and PVC (33 % w/w). 100 mg of the membrane cocktail was dissolved in 660 μL of THF. The weight ratios of the membrane ingredients were fixed at 1:0.55:65.45:33 [25]. The mixtures were vortexed to make a homogeneous solution. The MN Pt electrode was coated with 80 μL of the membrane cocktail and dried overnight.

2.8. Testing of the pH sensors

The stability and sensitivity of the pH electrodes were evaluated by assessing their response to changes in various pH buffers and to artificial ISF adjusted to different pH levels.

To conduct an interference study, a pH 5 solution was prepared, and 70 mM of NaCl, 15 mM of KCl, and 40 mM of $MgCl_2$ were added to the solution [32].

Open-circuit potential (OCP) measurements were carried out at room temperature to evaluate the potential electrode pH response. This assessment took place in a two-electrode electrochemical cell, with a MN electrode serving as the working electrode and an Ag/AgCl electrode as the reference electrode.

2.9. Testing of the Na^+ sensors

The stability and sensitivity of the Na^+ electrodes were evaluated by measuring the response to changes in differing NaCl concentrations; by the response to artificial ISF adjusted to differing NaCl concentrations. An interference study was conducted by preparing a solution of 200 mM NaCl and spiking the solution with 4 mM of KCl, 2.5 mM of $CaCl_2$ and 1 mM $MgCl_2$.

Square wave voltammetry (SWV) measurements were performed at a potential ranging from −0.9 to +0.4 V to evaluate the electrode Na^+ response at room temperature. This was conducted within a three-electrode electrochemical cell. A MN electrode was employed as the WE, a platinum wire as the counter electrode and an Ag/AgCl electrode was employed as the reference electrode. We used SWV because of the following surpasses OCP in electrochemical sensing with superior signal amplification, higher sensitivity, and faster analysis due to its differential measurement and pulsed waveform. It reduces capacitive currents, enhancing accuracy and signal-to-noise ratios. SWV effectively resolves closely spaced redox peaks, enabling direct analyte quantification, unlike OCP's qualitative insights. While OCP suits corrosion studies, SWV excels in redox-active species analysis. Its pulsed nature minimizes interference, improving selectivity, making SWV a more powerful and versatile technique for various sensing applications.

2.10. Microneedle sensors assembly

In Fig. 1, the process overview is illustrated. The microneedles were passivated with a variety of layers after being manufactured by micromoulding techniques previously reported by the group [33]. This paper focuses on two types of microneedle sensor. The first of these was passivated with SiO_2 and functionalised with iridium oxide via electrodeposition in order to produce MN sensors that were capable of detecting pH by OCP detection. Secondly, microneedles passivated with ARcare were functionalised with PEDOT via chronoamperometry and made selective to Na^+ by depositing a layer of the ion-selective membrane. These microneedle sensors were capable of detecting sodium via square wave voltammetry. Thus, successful microneedle sensors were demonstrated by the project design illustrated in Fig. 1.

3. Results and discussion

3.1. Characterisation of passivation layers

Ensuring protection from substrate interference and selectively exposing only the microneedle tip, passivating the microneedles becomes essential [30].

In Fig. 2, the voltammograms illustrate the potential peaks associated with the two different passivation processes, compared to a completely exposed MNs array. As expected, a smaller exposed area leads to lower observable currents, proving the efficacy of the passivation methods.

We analysed peak potential and current values for the oxidation and

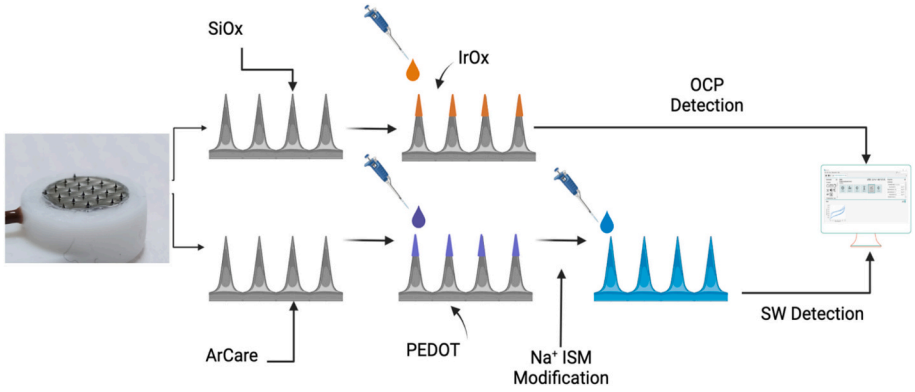

Fig. 1. Schematic layout of both the passivation and functionalisation of the MNs, coupled with their respective form of detection.

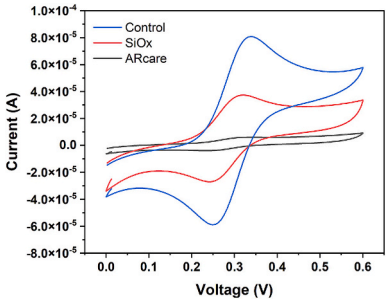

Fig. 2. CV scans performed in 1 mM of FcA after electrodes have been acid cleaned. Each graph represents the average of 12 MN samples of each respective passivation layer.

reduction processes of the redox couple, calculating the resulting half-wave potentials ($E_{1/2}$) and total currents (I).

The control electrode exhibits an $E_{1/2}$ value of 81 mV and current of 139.4 μA. In contrast, the passivated SiO_2 electrode's redox couple displays relatively lower values of $E_{1/2}$ and I: 64 mV and 63.9 μA respectively. Conversely, the passivated ARcare electrode has an $E_{1/2}$ of 66 mV, similar to the one reported for the passivated SiO_2, but a much lower current of 9.7 μA. These results are consistent with what expected as the exposed area is smaller from the control, to the passivated SiO_2 and to the passivated ARcare.

3.2. *Modification of the surface*

Modification of the MN is important for its functionality. Electrochemical deposition of iridium oxide on the electrode surface is performed to achieve complete functionalization. The quantity of iridium oxide required for measurements is determined by the extent of MN tip

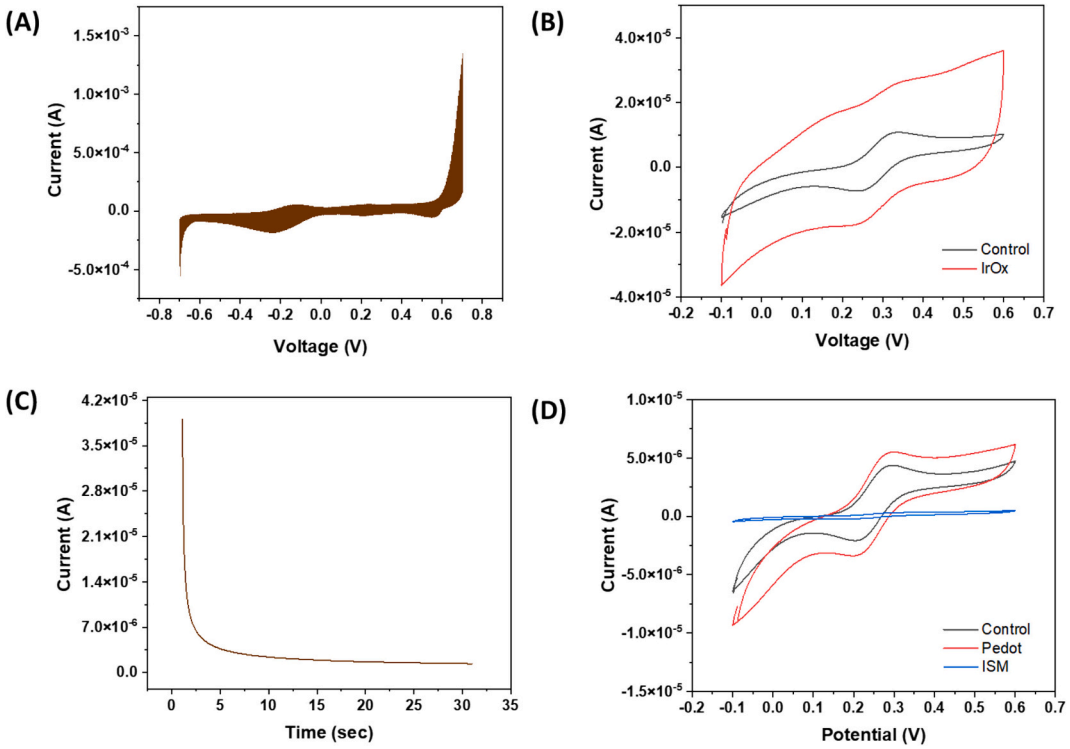

Fig. 3. (A) The deposition of Iridium Oxide on passivated SiO_2 samples at 10 scans via CV. (B) CV scan of passivated SiO_2 samples before deposition and after deposition in 1 mM FcA via CV. (C) The deposition of PEDOT on passivated ARcare samples for a duration of 30 s via CA. (D) CV scans of passivated ARcare samples before deposition, after deposition with PEDOT and after ISM was added in 1 mM of FcA.

exposure. Hence, optimizing the number of cyclic voltammetry (CV) scans for deposition is crucial (data not showed). Figs. 3A shows the deposition of the IrOx for passivated SiO_2 MN and Fig. 3B shows the scans before and after the deposition, demonstrating that a layer of IrOx was deposited on the surface of the MN.

To ensure the MN sensor's response to sodium, functionalization with PEDOT and an ion-selective membrane was conducted using chronoamperometry, as depicted in Fig. 3C and D. CV graphs in 1 mM of FcA (ferrocenylmethyltrimethylammonium) confirm the successful deposition of PEDOT and the ion-selective membrane. Following deposition, validation and detection studies were carried out. The sodium functionalized passivated ARcare MN samples were stored at room temperature.

In vitro investigations were conducted to characterize the developed sensors. Parameters such as detection, sensitivity, selectivity, and repeatability were established for the pH MN sensor and the Na^+ MN sensor over periods of 21 days and 14 days, respectively.

Fig. 3A shows the CV analysis of the formation of the IrOx layer on the surface, via electrodeposition, yielded an increase in current with an increasing number of cycles. Cyclic voltammetry was applied to study the electron transfer behaviour at the unmodified MN, following the IrOx electrodeposition (Fig. 3B) and the modification with PEDOT and ISM (see Fig. 3D). CV was carried out in 5 mM FcCOOH from −0.1 mV/s to +0.6 mV/s. The uniform surface coverage resulting from PEDOT modification is illustrated in Fig. 3C through the chronoamperometric response observed over a 30-s deposition period.

As shown in Fig. 3D, alterations in the peak-to-peak potential difference (ΔEp) and peak-to-peak current difference (ΔIp) of the FcCOOH are evident at each stage of the surface modification of MN. The unmodified MN exhibits a quasi-reversible electrochemical response for the FcCOOH, with ΔEp measuring 68 mV and ΔIp at 8.6 μA. Introducing PEDOT to the MN surface leads to a ΔEp increase of 2.8 mV and a ΔIp decrease of 2.3 μA.

Subsequently, introducing the ISM to the MN/PEDOT electrode surface induced alterations in the electrochemical behaviour of the FcCOOH redox, resulting in an increase in ΔEp by 42 mV and a decrease in ΔIp value by 6.2 μA.

3.3. Detection

The passivated SiO_2 MN samples were employed for open-circuit potential (OCP) detection to establish calibration graphs. The OCP values were plotted against various pH readings. The pH was changed using buffers at pH levels of 3, 5, 7, 9, and 11, and the accuracy of these values was verified using a benchtop calibrated pH meter. It's noteworthy that pH values outside this range are uncommon in the body, as the usual physiological pH range is 6.9 to 7.4 [9,15].

The sensors exhibited a good linear response, as illustrated in Fig. 4A. The passivated SiO_2 MN sensors displayed an excellent Nernstian response, registering −60.5 mV/pH on day 1; the data for day 7, 14 and 21 can be seen in Fig. S1A in the supplementary information. The sensitivity values of the passivated SiO_2 MN pH (−60.5 mV/pH) sensors align with those found in the literature [2,11,12]. The sensors exhibited an accuracy of 97.7 % alongside an error margin of 2.3 %, a shelf life of 21 days and 60s measurements.

Calibrating the sensor directly in the ISF matrix is crucial because it ensures that the electrode's response is tailored to the specific ionic composition and potential interferences present in the experimental environment. While buffer calibrations provide a foundational understanding of the electrode's behaviour, matrix-specific calibrations are necessary for accurate and reliable measurements in complex biological fluids.

Square wave voltammetry (SWV) was used to generate calibration graphs for MN ARcare passivation by plotting the highest peak point against the concentration, as depicted in Fig. 4B. Standard solutions ranging from 25 to 200 mM Na^+ were prepared to simulate

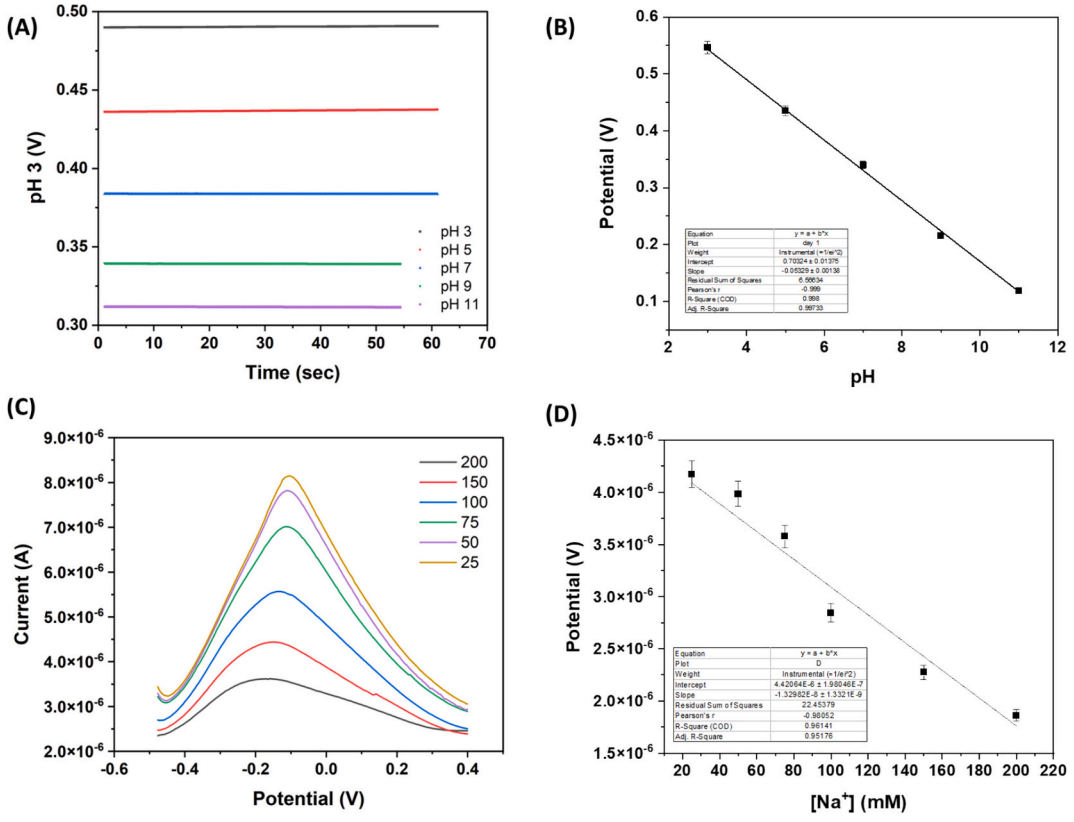

Fig. 4. (A) Calibration graphs generated for passivated SiO_2 pH MN sensors via OCP detection in pH buffers and (B) Calibration graphs for passivated ARcare Na^+ MN sensors via SWV detection in differing concentrations of NaCl. Each measurement was performed $n = 6$, error bars represent the standard error of the mean.

physiologically relevant conditions within the body. This approach resulted in achieving a sensitivity of 3.29 nA/mM/mm^2 in buffers with a 5 min reply form the sensor.

3.4. Interference and selectivity

As mentioned earlier, ISF encompasses numerous biomarkers. An interference study was conducted to assess the selectivity of the designed sensors toward their target biomarkers. A pH 5 solution was prepared and spiked with common interferents found in ISF [32]. Fig. 5A demonstrates that the sensors could selectively detect pH in the presence of interferents such as NaCl, KCl, and $MgCl_2$.

The most significant variance in OCP between the pH 5 solution (considered the control) and a solution spiked with an interferent was 0.025 V (Table 3). The interference study indicated a minor sensitivity to $MgCl_2$, possibly attributable to the solution's preparation, or due to the hydrolysis of magnesium cations and chloride anions, which can result in the formation of weakly basic magnesium hydroxide and hydrochloric acid or on other specific conditions of the solution, such as temperature, ionic strength, and presence of other substances. This sensitivity to $MgCl_2$ was also observed by Zuliani et al. [10] in their study. When examining the interference for pH 5 with KCl and NaCl, we observe values of 0.00780 V and 0.00087 V, respectively (Table 4).

The interference study design for the Na^+ sensors included 200 mM of NaCl solution spiked with interferents KCl, $MgCl_2$ and $CaCl_2$ (Fig. 5B), when evaluating the interference for NaCl, KCl, $MgCl_2$ and $CaCl_2$, we observe values of 7.38E-08 A, 3.47E-08 A, 3.02E-07 A and 1.26E-07 A, respectively (Table 4). The sensors demonstrated a good sensitivity compared with other ions; however, they began to lose selectivity to sodium on day 14. Perhaps leaving the newly modified sensors in a solution of NaCl for 8 h as Li et al. [25] demonstrated could improve the sensor performance. Evidently, the performance of these sensors must be studied and optimised further to maintain the stability and selectivity.

3.5. Reproducibility, sensitivity and stability

Calibration graphs for the passivated SiO_2 pH sensors and passivated ARcare sodium sensors were generated on day 1. In the subsequent weeks, the same passivated SiO_2 and passivated ARcare sensors were employed to conduct detection studies, assessing the stability of the sensors over an extended period. The sensors exhibited consistent linearity each week, the highest relative standard deviation value was 3.73 %, showing a slight variation but indicating repeatability in sensor responses. For the passivated SiO_2 MN, the R^2 values on day 1 and 7 were 0.9985 and 0.9947 respectively. Regarding the passivated Arcare MN, the R^2 values on days 1 and 7 were 0.8996 and 0.8615 respectively. Refer to Figs. S1A and S2B in the supplementary information for this data.

The variation for the pH sensors modified with iridium oxide is most likely introduced by the behaviour of iridium oxide. Iridium oxide pH sensors exist as Ir (III), Ir (IV) and Ir (V) oxides and the equilibrium between the oxides and the oxidation states may influence the performance of the sensors [34]. Rawson et al. [14] attribute the effect of non-conductive Ir (III) build up to the stability performance.

In Fig. 6A, the sensor stability was examined. A passivated SiO_2 sample was immersed in pH buffers 5, 7, 9, and 11 for 3 h. We observed a variation of less than 3.52 % in OCP during the microneedle immersion in the buffer solutions for 3 h.

In the subsequent study shown in Fig. 6B, a pH staircase was created, showcasing the sensors' ability to monitor dynamic pH changes in the body. Solutions of artificial ISF adjusted to pH 3, 5, 7, 9, and 11 were alternated every 60 s.

Table 3
Values of the selectivity coefficients between ions and the interference ions for pH sensor.

	Selectivity value (V)	Selectivity coefficient difference (V)
5	0.4222	*Target ion*
Na^+	0.42133	0.00087
K^+	0.41353	0.00780
Mg^{2+}	0.44707	0.02487

Table 4
Values of the selectivity coefficients between ions and the interference ions for Sodium sensor.

	Selectivity value (A)	Selectivity coefficient difference (A)
NaCl	1.11E-06	*Target ion*
Na^+	1.18E-06	7.38E-08
K^+	1.14E-06	3.47E-08
Mg^{2+}	1.41E-06	3.02E-07
Ca^{2+}	1.23E-06	1.26E-07

4. Conclusion

In conclusion, our study shows the development of microneedle sensors for pH and sodium detection, showcasing their potential as minimally invasive, point-of-care diagnostic tools. The successful creation of a polymer-based MN sensor, demonstrated through extensive in-vitro characterizations, marks a significant improvement toward future subcutaneous in-vivo electrochemical sensing. The sensor development for pH detection, employing SiOx as passivation layers with IrOx functionalization, as well as the achievement of sodium sensors with ARcare passivation, and PEDOT functionalization, underlines the versatility and adaptability of MN based technologies. Both pH and sodium sensors exhibit significant linear responses within normal physiological levels across diverse solutions, emphasizing their robustness.

Furthermore, the dynamic, rapid responses, good repeatability, and

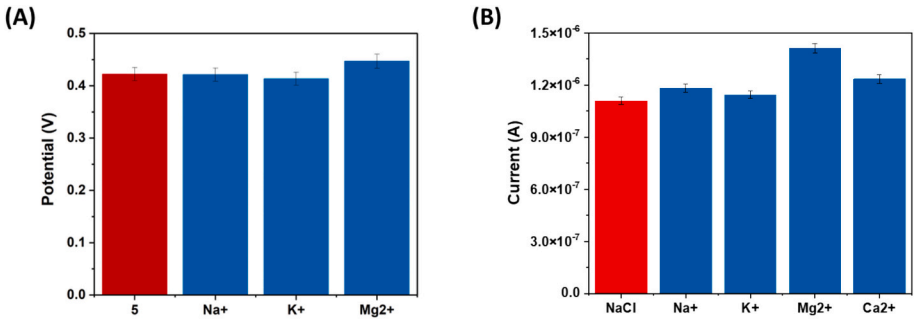

Fig. 5. (A) Demonstrates the interference study conducted for passivated SiO_2 MN samples over a period of 21 days for pH (B) Demonstrates the interference study conducted for passivated ARcare MN samples over a period of 14 days for Na^+. Each measurement was performed $n = 6$, error bars represent the standard error of the mean.

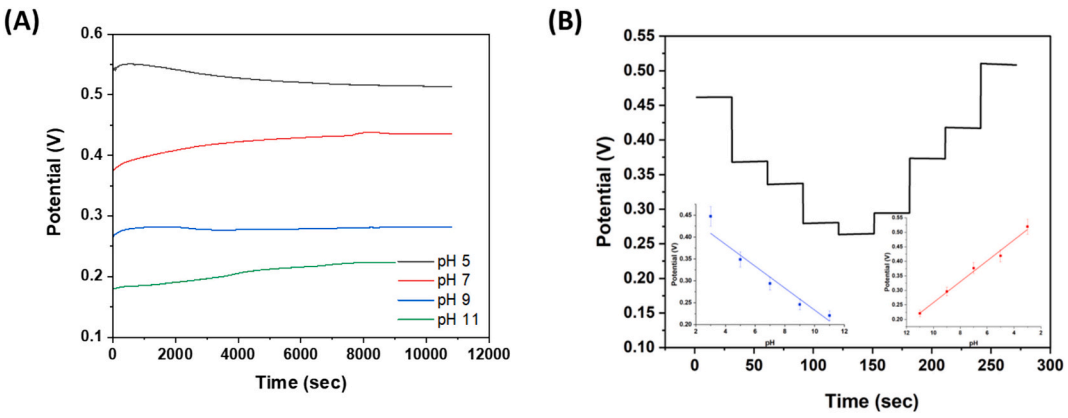

Fig. 6. (A) A SiO_2 sample was left in pH buffers 5, 7, 9 and 11 for 3 h. (B) SiO_2 sample was immersed in pH buffer 3, 5, 7, 9 and 11 for 60 s each to generate a pH staircase over 300 s.

selectivity demonstrated by both sensors over extended periods strengthen the case for the viability of microneedles as a foundation for wearable systems. The good Nernstian response of the pH sensors and the good sensitivity of the sodium sensors highlight the potential for real-time, multiparameter biosensing of interstitial fluids using this innovative approach.

In essence, this work shows a platform for the development of practical, wearable biosensing systems, for personalized healthcare and diagnostics.

Funding

This research was supported by Research Ireland (RI), through the Research Ireland Insight Centre for Data Analytics (SFI/12/RC/2289-P2).].

CRediT authorship contribution statement

Fahima Rahman: Investigation, Formal analysis. **Adam Ryan:** Investigation, Formal analysis, Data curation. **Andrea Bocchino:** Writing – original draft, Supervision. **Paul Galvin:** Resources, Funding acquisition. **Sofia Rodrigues Teixeira:** Writing – review & editing, Writing – original draft, Supervision, Conceptualization.

Declaration of competing interest

There are no conflicts of interest to disclose.

Acknowledgments

This publication has emanated from research supported in part by Research Ireland (RI), through the Research Ireland Insight Centre for Data Analytics (SFI/12/RC/2289-P2). For the purpose of Open Access, the author has applied a CC BY public copyright licence to any Author Accepted Manuscript version arising from this submission.

Data availability

The authors are unable or have chosen not to specify which data has been used.

References

[1] W.H. Choi, Fabrication of a needle-type pH sensor by selective electrodeposition, J. Micro/Nanolithogr. MEMS MOEMS 10 (2011) 020501.
[2] J.J. Guzmán, C.P. Ràfols, M. Cuartero, G.A. Crespo, Toward in vivo transdermal pH sensing with a validated microneedle membrane electrode, ACS Sens. 6 (2021) 1129–1137.
[3] W. Lee, S. Jeong, Y.W. Lim, H. Lee, J. Kang, H. Lee, I. Lee, H.S. Han, S. Kobayashi, M. Tanaka, B.S. Bae, Conformable microneedle pH sensors via the integration of two different siloxane polymers for mapping peripheral artery disease, Sci. Adv. (2025), https://doi.org/10.1126/sciadv.abi6290.
[4] Y. Zheng, R. Omar, R. Zhang, N. Tang, M. Khatib, Q. Xu, Y. Milyutin, W. Saliba, Y. Y. Broza, W. Wu, M. Yuan, H. Haick, A wearable microneedle-based extended gate transistor for real-time detection of sodium in interstitial fluids, Adv. Mater. 34 (2022) 2108607, https://doi.org/10.1002/adma.202108607.
[5] S.D. O'Donoghue, J.M. Dulhunty, H.K. Bandeshe, S. Senthuran, J.R. Gowardman, Acquired hypernatraemia is an independent predictor of mortality in critically ill patients, Anaesthesia 64 (2009) 514–520, https://doi.org/10.1111/j.1365-2044.2008.05857.x.
[6] H. Teymourian, F. Tehrani, K. Mahato, J. Wang, Lab under the skin: microneedle based wearable devices, Adv. Healthc. Mater. 10 (2021) 2002255, https://doi.org/10.1002/adhm.202002255.
[7] L. Ventrelli, L. Marsilio Strambini, G. Barillaro, Microneedles for transdermal biosensing: current picture and future direction, Adv. Healthc. Mater. 4 (2015) 2606–2640, https://doi.org/10.1002/adhm.201500450.
[8] X. Zhang, G. Chen, F. Bian, L. Cai, Y. Zhao, Encoded microneedle arrays for detection of skin interstitial fluid biomarkers, Adv. Mater. 31 (2019) 1902825, https://doi.org/10.1002/adma.201902825.
[9] Ganesh Kumar Mani, Kousei Miyakoda, Asuka Saito, Yutaka Yasoda, Kagemasa Kajiwara, Minoru Kimura, Kazuyoshi Tsuchiya, Microneedle pH sensor: direct, label-free, real-time detection of cerebrospinal fluid and bladder pH, ACS Appl. Mater. Interfaces 26 (2017) 21651–21659, https://doi.org/10.1021/acsami.7b04225.
[10] C. Zuliani, F.S. Ng, A. Alenda, A. Eftekhar, N.S. Peters, C. Toumazou, An array of individually addressable micro-needles for mapping pH distributions, Analyst 141 (2016) 4659–4666, https://doi.org/10.1039/C6AN00639F.
[11] J.X. Zhou, F. Ding, L.N. Tang, T. Li, Y.H. Li, Y.J. Zhang, H.Y. Gong, Y.T. Li, G. J. Zhang, Monitoring of pH changes in a live rat brain with MoS2/PAN functionalized microneedles, Analyst 143 (2018) 4469–4475, https://doi.org/10.1039/C8AN01149D.
[12] C. Hegarty, A. McConville, R.J. McGlynn, D. Mariotti, J. Davis, Design of composite microneedle sensor systems for the measurement of transdermal pH, Mater. Chem. Phys. 227 (2019) 340–346, https://doi.org/10.1016/j.matchemphys.2019.01.052.
[13] P. Steegstra, E. Ahlberg, Influence of oxidation state on the pH dependence of hydrous iridium oxide films, Electrochim. Acta 76 (2012) 26–33, https://doi.org/10.1016/j.electacta.2012.04.143.
[14] T.M. Rawson, S. Sharma, P. Georgiou, A. Holmes, A. Cass, D. O'Hare, Towards a minimally invasive device for beta-lactam monitoring in humans, Electrochem. Commun. 82 (2017) 1–5, https://doi.org/10.1016/j.elecom.2017.07.011.
[15] S.M. Mugo, W. Lu, M. Wood, S. Lemieux, Wearable microneedle dual electrochemical sensor for simultaneous pH and cortisol detection in sweat, Electrochem. Sci. Adv. 2 (2022) e2100039, https://doi.org/10.1002/elsa.202100039.
[16] Marc Parrilla, Andres Vanhooydonck, Maby Johns, Regan Watts, Karolien De Wael, 3D-printed microneedle-based potentiometric sensor for pH monitoring in skin interstitial fluid, Sensors Actuators B Chem. 378 (2023) 133159, https://doi.org/10.1016/j.snb.2022.133159.
[17] Yevedzo Chipangura, Maria Komal, Vilma S.M. Brandao, Christopher Sedmak, Jung Suk Choi, Sarah L. Swisher, Philippe Bühlmann, Andreas Stein, Nanoporous carbon materials as solid contacts for microneedle ion-selective sensors, ACS Appl. Mater. Interfaces 16 (34) (2024) 44428–44439.
[18] Águeda Molinero-Fernandez, Qianyu Wang, Xing Xuan, Åsa Konradsson-Geuken, Gastón A. Crespo, María Cuartero, Demonstrating the analytical potential of a wearable microneedle-based device for intradermal CO_2 detection, ACS Sensors 9 (1) (2024) 361–370, https://doi.org/10.1021/acssensors.3c02086.
[19] Marc Parrilla, Annemarijn Steijlen, Robbe Kerremans, Joe Jacobs, Louise den Haan, Janne De Vreese, Yorben Van Noten, Phil Clerx Géron, Regan Watts, Karolien De Wael, Wearable platform based on 3D-printed solid microneedle

potentiometric pH sensor for plant monitoring, Chem. Eng. J. 500 (2024) 157254, https://doi.org/10.1016/j.cej.2024.157254.
[20] L. Hamm, L. Hering-Smith, K.S. Nakhoul, N. L., Acid-base and potassium homeostasis, Semin. Nephrol. 33 (2013) 257–264, https://doi.org/10.1016/j.semnephrol.2013.04.006.
[21] J. Terry, The major electrolytes: sodium, potassium, and chloride, J. Intraven. Nurs. 17 (1994) 240–247.
[22] G.B. Piccoli, M. Capobianco, L. Odetto, M.C. Deagostini, V. Consiglio, G. Radeschi, Acute renal failure, severe sodium and potassium imbalance and sudden tetraplegia, NDT Plus 3 (2010) 247–252, https://doi.org/10.1093/ndtplus/sfq017.
[23] C.V. Leier, L. Dei Cas, M. Metra, Clinical relevance and management of the major electrolyte abnormalities in congestive heart failure: hyponatremia, hypokalemia, and hypomagnesemia, Am. Heart J. 128 (1994) 564–574, https://doi.org/10.1016/0002-8703(94)90633-5.
[24] S.P. Von Duvillard, W.A. Braun, M. Markofski, R. Beneke, R. Leithäuser, Fluids and hydration in prolonged endurance performance, Nutrition 20 (2004) 651–656, https://doi.org/10.1016/j.nut.2004.04.011.
[25] Huijie Li, Wu Guangfu, Zhengyan Weng, He Sun, Ravi Nistala, Yi Zhang, Microneedle-based potentiometric sensing system for continuous monitoring of multiple electrolytes in skin interstitial fluids, ACS Sens. 6 (2021) 2181–2190, https://doi.org/10.1021/acssensors.0c02330.
[26] P. Pirovano, M. Dorrian, A. Shinde, A. Donohoe, A.J. Brady, N.M. Moyna, G. Wallace, D. Diamond, M. McCaul, A wearable sensor for the detection of sodium and potassium in human sweat during exercise, Talanta 219 (2020) 121145, https://doi.org/10.1016/j.talanta.2020.121145.
[27] A.M. Zamarayeva, A. Toor Natasha, M.E. Payne, C. Woods, V.I. Pister, Y. Khan, J. W. Evans, Ana Claudia Arias, Optimization of printed sensors to monitor sodium, ammonium, and lactate in sweat, APL Mater. 8 (2020) 100905, https://doi.org/10.1063/5.0014836.
[28] Águeda Molinero-Fernandez, Ana Casanova, Qianyu Wang, María Cuartero, Gastón A. Crespo, In vivo transdermal multi-ion monitoring with a potentiometric microneedle-based sensor patch, ACS Sens. 8 (1) (2023) 158–166, https://doi.org/10.1021/acssensors.2c01907.
[29] P. Bollella, S. Sharma, A.E.G. Cass, F. Tasca, R. Antiochia, Minimally invasive glucose monitoring using a highly porous gold microneedles-based biosensor: characterization and application in artificial interstitial fluid, Catalysts 9 (2019) 580, https://doi.org/10.3390/catal9070580.
[30] A. Bocchino, S.R. Teixeira, S. Iadanza, E. Melnik, S. Kurzhals, G.C. Mutinati, C. O'Mahony, 44th Annual International Conference of the IEEE Engineering in Medicine & Biology Society (EMBC), 2022, https://doi.org/10.1109/embc48229.2022.9871005. 36.
[31] K. Yamanaka, Anodically electrodeposited iridium oxide films (AEIROF) from alkaline solutions for electrochromic display devices, Jpn. J. Appl. Phys. 28 (1989) 632–637.
[32] L.Q. Wu, K. Lee, X. Wang, D.S. English, W. Losert, G.F. Payne, Chitosan mediated and spatially selective electrodeposition of nanoscale particles, Langmuir 21 (2005) 3641–3646, https://doi.org/10.1021/la047420c.
[33] C. O'Mahony, Design, fabrication and skin-electrode contact analysis of polymer microneedle-based ECG electrodes, J. Micromech. Microeng. 26 (July 2016) 084005, https://doi.org/10.1088/0960-1317/26/8/084005.
[34] P.R. Miller, S.A. Skoog, T.L. Edwards, D.M. Lopez, D.R. Wheeler, D.C. Arango, X. Xiao, S.M. Brozik, J. Wang, R. Polsky, R.J. Narayan, Multiplexed microneedle-based biosensor array for characterization of metabolic acidosis, Talanta 88 (2012) 739–742, https://doi.org/10.1016/j.talanta.2011.11.046.